Novel Explant Model to Study Mechanotransduction and Cell–Cell Communication

C. Edward Hoffler, Kurt D. Hankenson, Joshua D. Miller, Sukhinderdeep K. Bilkhu, Steven A. Goldstein

Orthopaedic Research Laboratories, Department of Orthopaedic Surgery, The University of Michigan, 2003, Biomedical Science Research Building, Ann Arbor, Michigan 48109-2200

Received 2 November 2005; accepted 2 March 2006

Published online 20 June 2006 in Wiley InterScience (www.interscience.wiley.com). DOI 10.1002/jor.20207

ABSTRACT: To understand in situ behavior of osteocytes, we characterized a model of osteocytes in their native bone matrix and demonstrated real-time biologic activity of osteocytes while bending the bone matrix. Using 43 male Sprague-Dawley rats, dumbbell-shaped explants were harvested from stainless steel femoral implants after 6–12 weeks and incubated in culture medium or fixed. Sixteen specimens were used to determine bone volume density (BV/TV), volumetric bone mineral density (BMD) and histology for different implantation periods. Osteocyte viability was evaluated by L-lactate dehydrogenase (LDH) activity in 12 cultured explants. Confocal microscopy was used to assess tracer diffusion in three explants and changes in osteocyte pH of a mechanically loaded explant. From 6 to 12 weeks, explant BV/TV and volumetric BMD trended up 92.5% and 101%, respectively. They were significantly and highly correlated. Tissues were uniformly intramembranous and all bone cell types were present. Explants maintained LDH activity through culture day 8. Diffusion at 200 μM was limited to 1,209 Da. Explants appeared capable of reproducing complex bone biology. This model may be useful in understanding osteocyte mechanotransduction in the context of a physiologically relevant bone matrix. © 2006 Orthopaedic Research Society. Published by Wiley Periodicals, Inc. J Orthop Res 24:1687–1698, 2006

Keywords: rodent; bone; biomechanics; mechanical loading; implant

INTRODUCTION

In an effort to understand age-related increases in bone fragility, numerous investigators have begun to explore the relationship between bone extracellular matrix (ECM) mechanics and osteocyte physiology. For example, bone matrix microcracks were found to be more prevalent in aging adults.[1–3] Moreover, these microcracks occurred in the femoral neck,[3] which was one of the primary locations of age-related fragility fractures.[4,5] These data indicated that changes in bone ECM mechanical integrity might be factors in the etiology and pathogenesis of these fractures.

Osteocytes are embedded in bone matrix and ideally situated to sense the bone mechanical environment via. mechanosensation may occur via bone matrix or canalicular fluid interactions with osteocyte soma or processes. Studies have collectively linked osteocyte injury and death with bone microcracks, fatigue loading and subsequent bone resorption.[6–10] We consider bone matrix to be an important medium through which osteocytes perceive physical phenomena. Therefore, cell physiology may be dramatically altered in experimental systems which lack native mineralized extracellular matrix. Unfortunately, techniques to study osteocytes in situ, i.e., surrounded by normal bone matrix, and under controlled mechanical conditions are limited and difficult to develop.

Current experimental approaches to exploring osteocytes and bone matrix strains have included animal studies with implants[11–16] or external loading devices,[9,17–22] bone biopsy culture[23–28] and bone organ culture.[24,28] The primary mechanical limitation of these models was an inability to calculate strains in bone matrix around osteocytes. Based on applied loads and possibly measured surface strains, bone strains could be estimated using organ level analyses like strength of materials and finite element methods. These techniques required architectural simplifications, material property estimates, and constitutive behavior assumptions that made accurate prediction of pericellular bone matrix strains challenging. Biologically, biopsies were limited by the need to extensively sever the canalicular network, which may be critical to osteocyte mechanosensation. Bone organ models bypassed this issue, but still

Correspondence to: Steven A.Goldstein (Telephone: 734-936-7417; Fax: 734-647-0003; E-mail: stevegld@umich.edu)

needed to contend with irregular structures for mechanical testing and strain characterization.

The purpose of this study was to characterize a novel model of osteocytes embedded in their native three-dimensional extracellular matrix, which could facilitate real-time measurements of osteocyte biologic activity during controlled mechanical loading.

MATERIALS AND METHODS

Implant Description

The implants were made of corrosion resistant type 303 or type 304 stainless steel as shown in Figure 1A. The first component was a base plate (2.49 mm × 3.15 mm × 0.51 mm) with two open parallel channels shaped like dumbbells. Channels were 794 μm wide by 254 μm deep and were designed to permit tissue in-growth. The channel base plate had a central tapped hole so that fastening this component to a cover plate could cover the channels. The cover plate was a 14 mm × 4 mm × 0.25 mm component with three holes spaced by 5.5 mm and centered on the part. The central hole in the cover plate enabled attachment to the channel base plate using a #000-120 machine screw (J. I. Morris Co., Southbridge, MA) and washer (not shown). The two peripheral holes in the back plate allowed the fully assembled implant to be surgically secured to the femoral defect site.

Model Description

The surgical model employed adult male Sprague-Dawley rats and bilateral placement of stainless steel implants in the femoral diaphyses. Animal use was approved by University Committee on Use and Care of Animals. Rats were obtained from Harlan and Charles River Laboratories, and preoperative weights varied from 390 to 500 g with a 455 g mean. General anesthesia was induced with 2% isofluorane in a chamber and subsequently maintained via mask. Subsequent to induction, animals received 5 ml of warmed lactated Ringer's solution mixed with butorphenol (1 mg/kg) followed by atropine (0.1 mg/kg) subcutaneously as a bolus. Finally, the lower extremities were shaved and prepared for aseptic surgery with ethanol and chlorhexadine (Vetpo Distributors, Holland, Michigan).

The anterolateral femoral diaphysis was approached through a lateral 2 cm incision, which passes through the lateral intermuscular septum. After elevating the periosteum, a small bur (Sullivan-Schein Dental) was used to create a (2.49 mm × 3.15 mm) rectangular defect in the anterolateral cortex. The dimensions were verified using a custom-sizing template. Next, the implant was fitted to the diaphysis with the channel base plate suspended in the defect and the cover plate resting on the periosteal surface of the femur. The implant was secured by placing self-tapping screws through predrilled holes in both cortices. The cover plate served to hold the implant within the defect and provide biomechanical support to

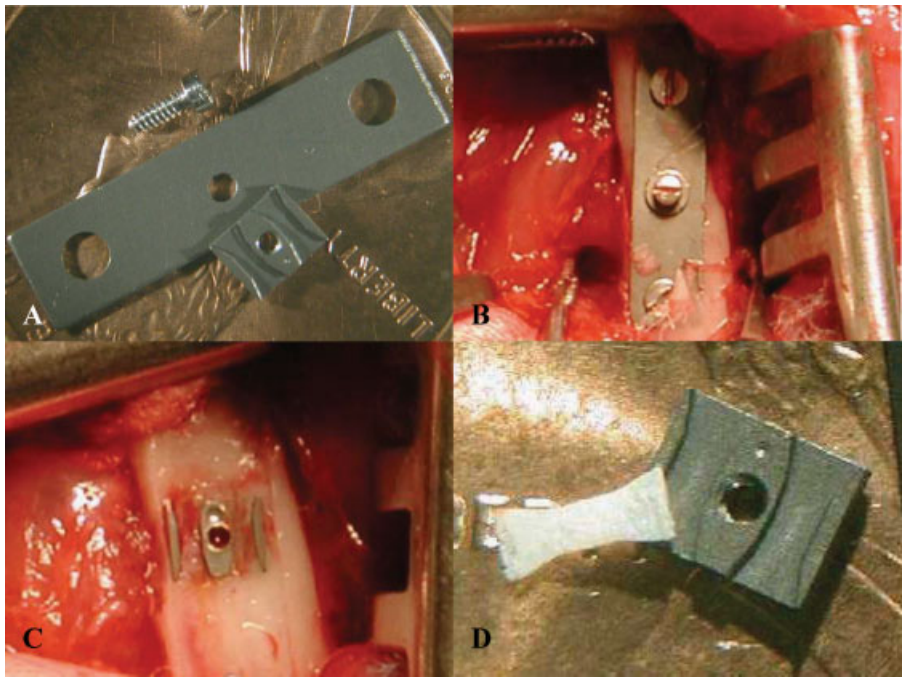

Figure 1. Implant and explant surgical model. (A) Implant cover plate was attached to channel side of chamber via machine screw. United States penny backdrop shown for scale. (B) Implant was exposed via a lateral incision and often was partially obscured with bony overgrowth. (C) Cover plate was removed to reveal implant with bone filling in-growth channels. (D) Representative specimen. [Color scheme can be viewed in the online issue, which is available at http://www.interscience.wiley.com]

 DOI 10.1002/jor

the femur. The wound was flushed with saline, closed in layers, and the skin was stapled. The procedure was then repeated on the contralateral limb. The implant functioned like an internal fixation device and helped prevent postimplantation fractures. Radiographs were taken immediately postoperatively, and animals were recovered in a heated environment. The implantation period varied from 6 to 12 weeks.

At harvest, animals were anesthetized and, under sterile conditions, the implant was exposed through the original lateral approach (Fig. 1B). Then the cover plate was removed to expose the explant specimens embedded in the bone (Fig. 1C). The chamber and explants were extracted en bloc with custom elevators and placed in culture media or fixative. Explants were removed from the chamber with a number 11 scalpel blade within 10 min (Fig. 1D). After repeating the extraction for the contralateral limb, animals were euthanized intraoperatively with intracardiac sodium pentobarbital (100 mg/kg).

Specimens for culture were directly transferred to an incubator at 37°C with 5% CO_2, and harvest media was replaced with fresh media within 3 h. Explants were cultured in BGJb (Fitton-Jackson modification) with 10% heat-inactivated fetal bovine serum, penicillin (100 U/ml), streptomycin (100 μg/ml), amphotericin B (5 μg/ml), and daily ascorbic acid (75 μg/ml) (all products from Invitrogen).[29]

Microcomputed Tomography Analysis

Specimens were separated from adherent soft tissue at harvest, fixed immediately in 10% neutral buffered formalin for at least 8 h and stored in 70% ethanol to await further processing. Micro computed tomography (micro CT) was used to evaluate specimen mineralization and morphology by quantifying bone mineral density (volumetric BMD) and bone volume fraction (BV/TV). Subsequently, specimens were prepared for routine histology.

MicroCT analysis was performed using 10 μm voxels (GE Medical Systems). Data were calibrated to air, water, and bone standards provided by the manufacturer. Mineralized and unmineralized tissues were thresholded based on minima in histograms of specimen gauge sections. Volumetric BMD and BV/TV were calculated for the gauge sections (narrow region of explants) of the specimens. BV/TV was computed as the number of bone voxels within the gauge section divided by the volume of the gauge section. Volumetric BMD was computed as the mineral mass present within the gauge section divided by the gauge section volume. Note that the units of volumetric BMD were g/cm^3 and were distinct from BMD measured by DEXA, which has units of g/cm^2. Mineral mass was quantified from grayscale values calibrated to the standards described above. For each specimen, gauge section volume was measured from the thresholded data. Six-week and 12-week results were compared using a t-test with p values less 5% indicating statistical significance. Given that there was random variation in the implant manufacturing process, implant stiffness also varied. Specimen thickness was measured as a proxy for channel base plate compliance. Its effect on BV/TV was evaluated using linear regression analysis.

Histologic Analysis

Specimens were decalcified in formic acid buffered with sodium citrate, embedded in paraffin, sectioned at 7 μm and stained with alcian blue hematoxylin and acid fuchsin eosin.

For quantitative histology, three 7-μm-thick sections spanning the central 100-μm thickness of each specimen were examined. Sections were separated by 50 μm. Explants were processed to produce dumbbell-shaped sections. Images of the gauge region were captured at ×100 using light and polarized light microscopy. Two adjacent fields were sufficient to span this area. Lamellar and woven tissue areas were measured using Bioquant Nova 4.00 image analysis software (R&M Biometrics, Inc.). Percent lamellar tissue area was calculated as lamellar tissue area divided by total measured tissue area. Lamellar tissue area was characterized as a function of implantation period and of specimen thickness. Finally, one-way ANOVA was used to explore implantation period results, and linear regression analysis was performed on thickness data.

Viability Analysis

L-lactate dehydrogenase (LDH) activity was assayed as a measure of cell viability. Specimens were decalcified in 10% EDTA with 0.1 M Tris (pH 7.0) at 4°C for 25 h. Next explants were washed in 2.5 mM phosphate buffer (pH 7.2) and then incubated at 37°C for 4.5 h in L-lactate dehydrogenase labeling medium.[30] (All reagents available from Sigma-Aldrich). After labeling, specimens were fixed for 25 min in 10% neutral buffer formalin, dehydrated with an ethanol series, transferred to xylene, mounted and coverslipped. Gauge segments were qualitatively evaluated with ×40 and ×100 light microscopy for formazan deposits in lacunae, which indicated cell viability.

Diffusion Analysis

We observed diffusion of polar tracers with a Zeiss LSM 510 Laser Scanning Confocal Microscope mounted on a Zeiss Axiovert 100M inverted microscope (Carl Zeiss, Inc.). Three explants were harvested and cultured as previously described. Experiments were initiated a minimum of 24 h after changing media. Using Tyrode's solution, each specimen was incubated for 2 h in 200 μM Alexa Fluor 633 hydrazide (~950 Da) and 200 μM Alexa Fluor 546 biocytin (1,209.7 Da) (Molecular Probes). Excitation wavelengths were 633 nm and 543 nm, respectively, with a 1.8 μm optical thickness. Scans were performed approximately 45 μm from the tissue surface, near the limit of optical penetration.

RESULTS

Model Characterization

Forty-three rats have undergone the implant–explant protocol and generally tolerated the procedure well, returning to normal cage activity within 30 min. Four animals were euthanized due to intraoperative or postoperative complications (diaphyseal fractures caused by stress risers created when cutting the cortical window). In unfractured femora, 74% of channels yielded complete bone specimens, and 8% were partially filled with bony tissue. The balance of channels was either filled with immature uncalcified tissue or empty. A representative dumbbell specimen is illustrated in Figure 1D.

The implant design provided (1) a biocompatible corrosion resistant material, (2) an implant stiffness that could be controlled by changing channel base plate thickness, (3) a flexible channel geometry, and (4) components that were readily available and inexpensive. The implant was completely internal which prevented infection and mechanical trauma often associated with external fixation. "Engineered" living bone specimens were produced in shapes specific to conventional mechanical testing regimens. Specimens were sufficiently thin and flat to facilitate confocal microscopy and prolonged tissue culture. Finally, the two-component implant could be disassembled to permit a less traumatic extraction than was likely possible if one were to cut a bony specimen from live tissue. Specifically, this meant that less osteocyte processes were severed and more native cell–cell communication and mechanosensation were preserved.

Implant Period Analysis

To determine the period required for tissue ingrowth and maturation, explants from four groups of four animals were harvested at 6, 8, 10, and 12 weeks following implantation. Specimens became more consolidated from 6 to 12 weeks (Fig. 2). In fact, typical 6-week specimens were too fragile and unmineralized to harvest intact. Mid-coronal and transverse sections demonstrated that while much of the fine porosity decreased over time, specimens never became fully dense bone (Fig. 2). Twelve-week samples had relatively flat surfaces, making them suitable for optical analysis with laser scanning confocal microscopy. Twelve-week specimens also appeared more radiopaque than the earlier specimens, indicating their advanced stage of mineralization.

BV/TV increased 92.5% from 20.0% at 6 weeks to 38.5% at 12 weeks, which was nearly significant with $p = 0.052$ (Fig. 3A). Volumetric BMD had a similar increase of 101% from 194 mg/ml to 390 mg/ml with $p = 0.080$ (Fig. 3B). Volumetric BMD and BV/TV were highly correlated with $R = 0.88$ and $p < 0.001$ (Fig. 4A). Neither volumetric BMD (data not shown) nor BV/TV (Fig. 4B) correlated significantly with specimen thickness ($p = 0.285$ and 0.170, respectively).

All micro CT specimens were processed for histology, stained with alcian blue hematoxylin and acid fuchsin eosin, and qualitatively evaluated for tissue origin, organization, mineralization, and resident cell types. Endochondral tissues were defined by a deep purple hue often with embedded chondrocytes identified as clusters of uniform cells with large nuclei and abundant cytoplasm. Intramembranous tissue was distinguished by its pink matrix with canaliculi, irregular collagen organization, and an irregular distribution of embedded osteocytes with cytoplasmic processes. Histologic data were consistent with micro CT. Tissue volume increased, but explants did not form dense compact bone (Fig. 5A). For all implantation periods, most of the non-osseous tissue was a hypercellular marrow, which was observed in several specimens but was often lost during histologic processing. Occasionally there was fibrous tissue (disorganized collagenous matrix with many fibroblastic cells) within the bony structure and at the implant interface.

Cartilage was not observed in any of the specimens suggesting the tissue was uniformly intramembranous. Occasionally, there were intramembranous tissues that weakly stained with alcian blue suggesting that cartilaginous molecules were present in an otherwise intramembranous morphology. Microstructurally, the tissue was a mixture of woven and lamellar bone (see Fig. 5B and C). The specimens were generally composed of more woven than lamellar bone. Lamellar bone was most often observed near the implant surfaces as would be expected from surface remodeling.

All bone cell types were present. The overwhelming majority were osteocytes, identified by their position within lacunae. Bone lining cells were often present at the implant interface. Osteoblasts were readily apparent as cuboidal cells adjacent to pale osteoid matrix but were not on the majority of surfaces. Their population peaked slightly at 8 weeks and then decreased below 6-week levels. Osteoclasts were generally not visible, but they were present in several 12-week explants. By 8 weeks, there was rare osteonal

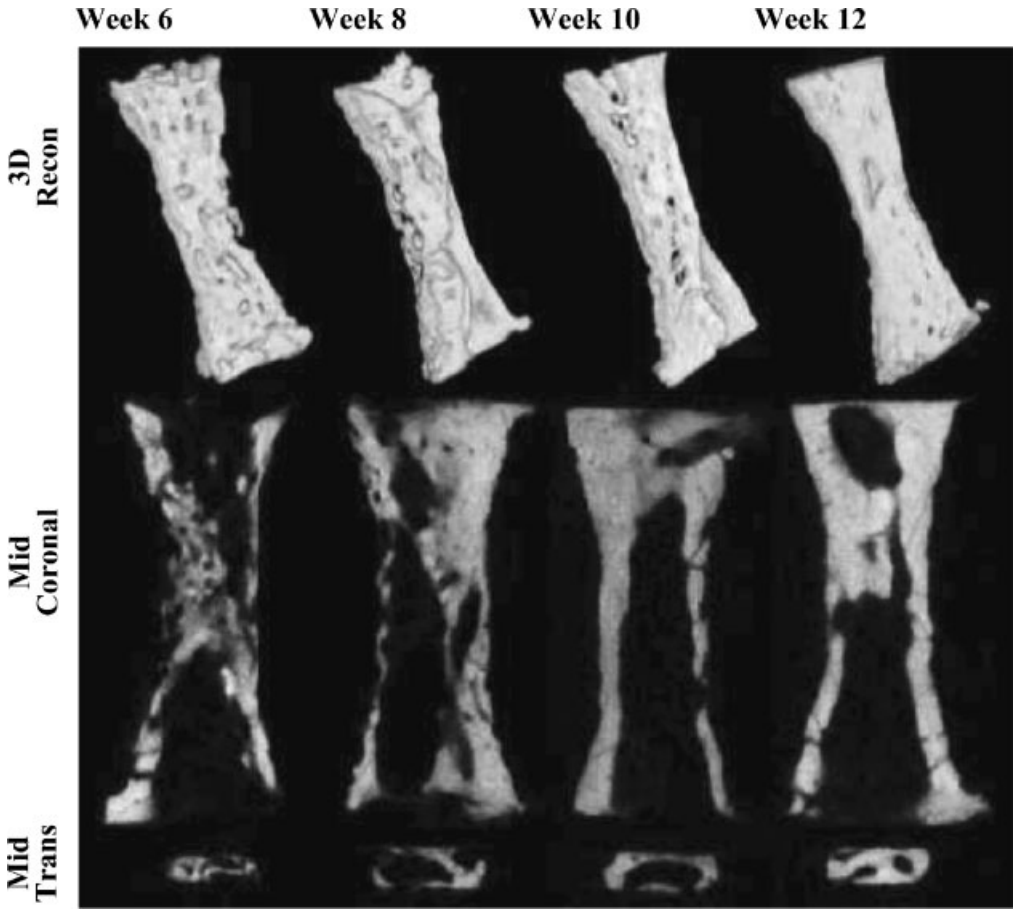

Figure 2. Specimens harvested after different implantation periods and imaged at 10 μm resolution with microcomputed tomography. 3D Recon = three dimensional reconstruction; Mid Coronal = middle coronal section; Mid Trans = middle transverse section. Specimens are approximately 2.5 mm in length.

remodeling which became more common by 10 and 12 weeks.

After qualitative studies, all explant specimens were examined quantitatively to determine: (1) whether the fraction of lamellar tissue increased as implantation period increased, and (2) if variations in implant stiffness could explain variations in lamellar tissue quantities. First, we evaluated lamellar tissue area changes during implantation to assess whether the explants were progressing to a mature state of mostly lamellar tissue. Secondly, we wanted to determine if the variations in implant stiffness were driving bone apposition or remodeling. Lamellar tissue area did not increase significantly with longer implantation periods ($p = 0.32$) (data not shown). Week 6 values increased from $0.5 \pm 1.1\%$ (±standard deviation) to 6.9 ± 8.7 at week 12. Lamellar tissue area increased with specimen thickness (a proxy for implant compliance). The correlation was significant ($p = 0.033$), but not strong ($R^2 = 30.4\%$) (data not shown).

Ex Vivo Tissue Viability Analysis

L-lactate dehydrogenase (LDH) activity was assessed as a measure of cell viability. Twelve-week explant specimens were harvested and placed in culture as described earlier. Three specimens were cultured for each of the following time periods: 0, 2, 5, and 8 days.

Osteocytes remained viable in tissue culture through day 8. Cells throughout the central gauge section contained formazan precipitate indicating LDH activity and osteocyte viability (Fig. 6). The presence of formazan deposits was consistent with positive control assays of freshly harvested murine metacarpals and distinctly different from the absence of staining in negative controls treated with KCN (data not shown).

Diffusion Analysis

To estimate the molecular weight threshold for probe diffusion, polar tracer diffusion was studied

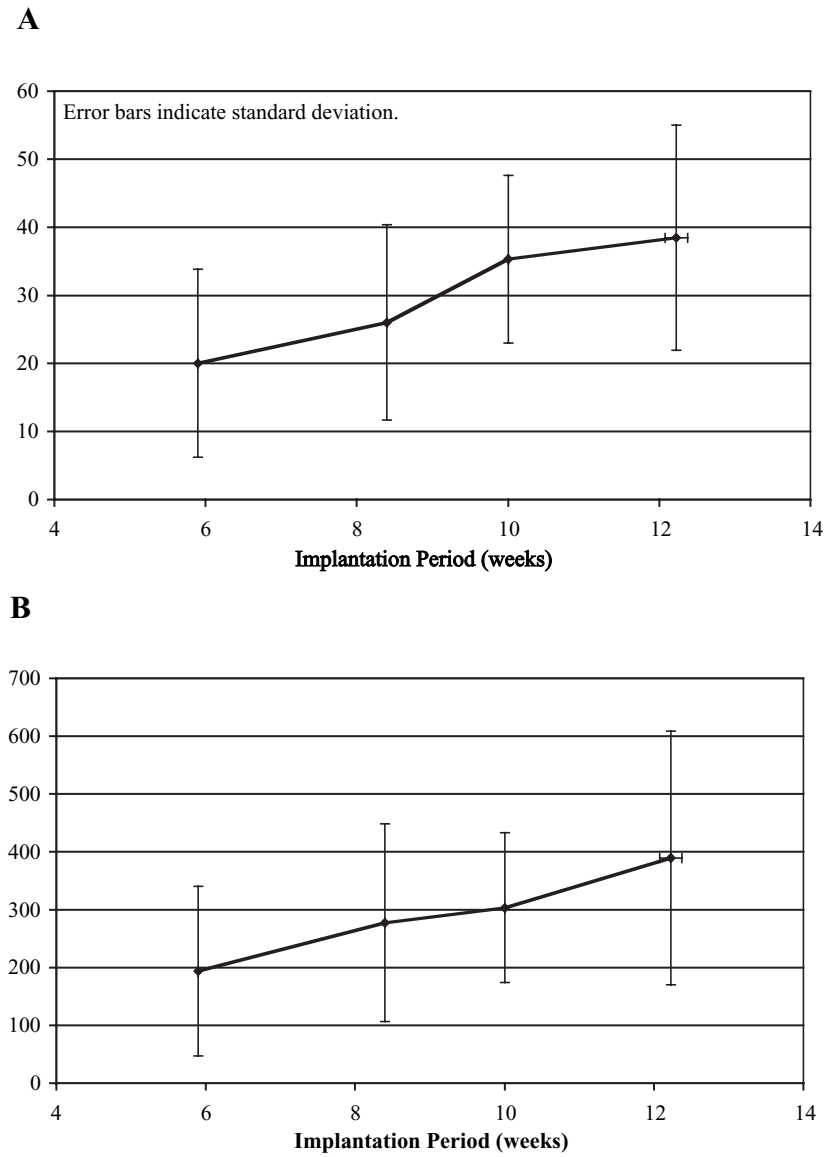

Figure 3. Bone mineral density and bone volume fraction. (A) Bone volume fraction as a function of implantation period. (B) Bone mineral density as a function of implantation period.

using confocal microscopy. Probe molecular weights were selected based on recent literature[31] and previous experience with cell labeling. The confocal micrograph in Figure 7A demonstrated that the 950 Da tracer had accessed osteocyte lacunae within 10 min. The tracer was spreading from the lower right hand corner of the field and was located diffusely within the matrix and more focally in lacunae and canaliculi. Diffusion via lacuno-canalicular network appears to be occurring faster than via matrix microporosity. Extracellular tracer exclusion was visible as a bright signal along lacunae perimeters. By 2 h, diffuse matrix labeling was much less visible, and more lacunae were filled with tracer (Fig. 7B). In contrast, the 1,209.7 Da tracer did not advance beyond the initial background fluorescence visible after 10 min (Fig. 7C and D). There was no specific lacunar localization even after 2 h.

Subsequently, carboxyfluorescein diacetate (CFDA, 532.46 Da; Molecular Probes) was introduced as a fluorescent H^+ indicator and verified with confocal microscopy in preparation for future real-time intracellular pH change measurements (data not shown).

 DOI 10.1002/jor

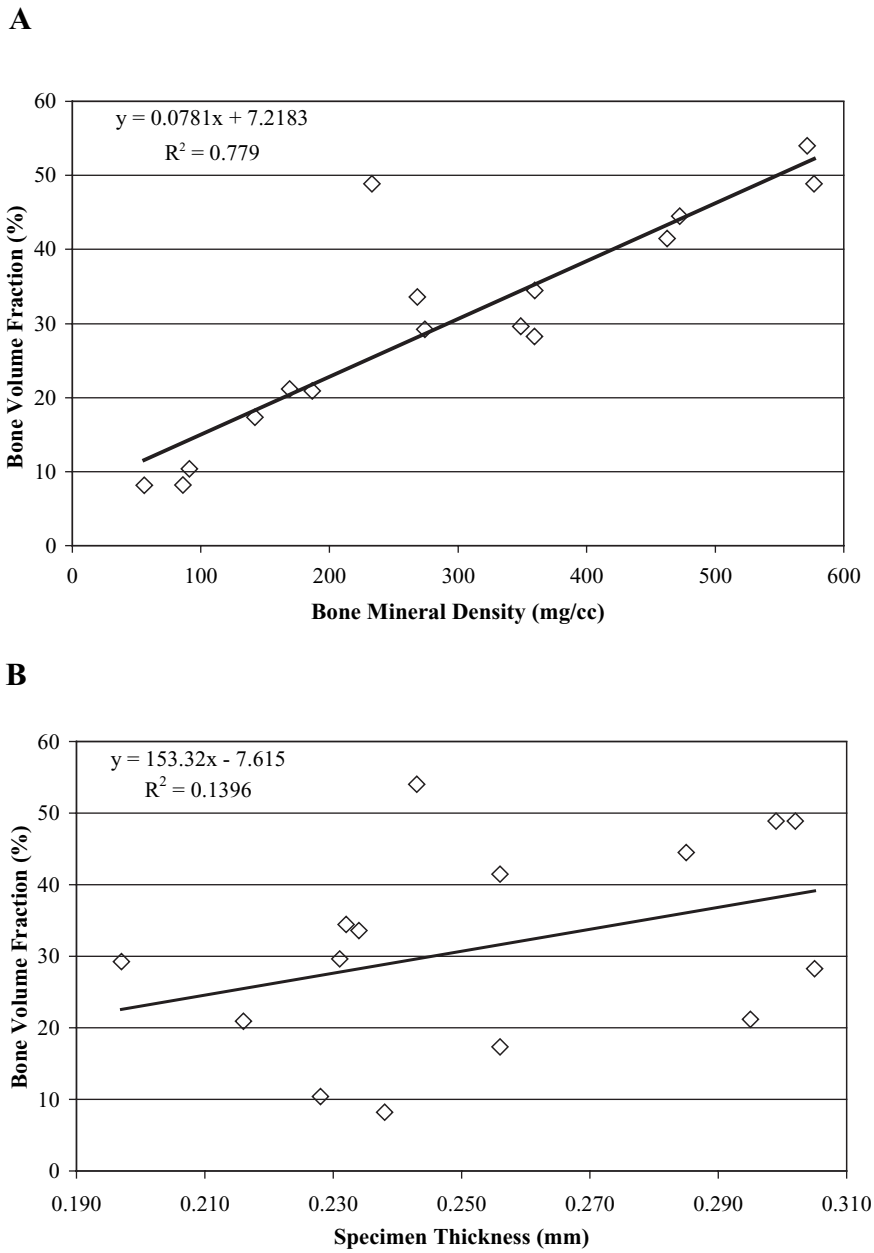

Figure 4. Additional bone mineral density and bone volume fraction analyses. (A) Significant correlation between bone mineral density and bone volume fraction ($p < 0.001$). Note that in the absence of datum at BMD = 233, the regression changed to $\mathrm{BV/TV} = 0.0815 \times \mathrm{BMD} + 4.6407$ with $R^2 = 0.9513$. (B) Bone volume fraction as a function of specimen thickness ($p = 0.170$).

DISCUSSION

Osteocytes are postulated to play a mechanosensory role in the maintenance of bone and potentially in the etiology and pathogenesis of age-related bone fragility. Progress in investigating the mechanisms associated with mechanosensation has been hampered by the absence of models enabling the microscopic study of the interaction of osteocytes while embedded within their native bone matrix. We consider bone ECM to be a medium through which osteocytes perceive physical phenomena, and mechanotransduction may be altered in experimental systems which lack native mineralized extracellular matrix. Moreover, traditional cell culture models have flat substrate cell-matrix interactions, which differ from three-dimensional systems, and have distinct biologic

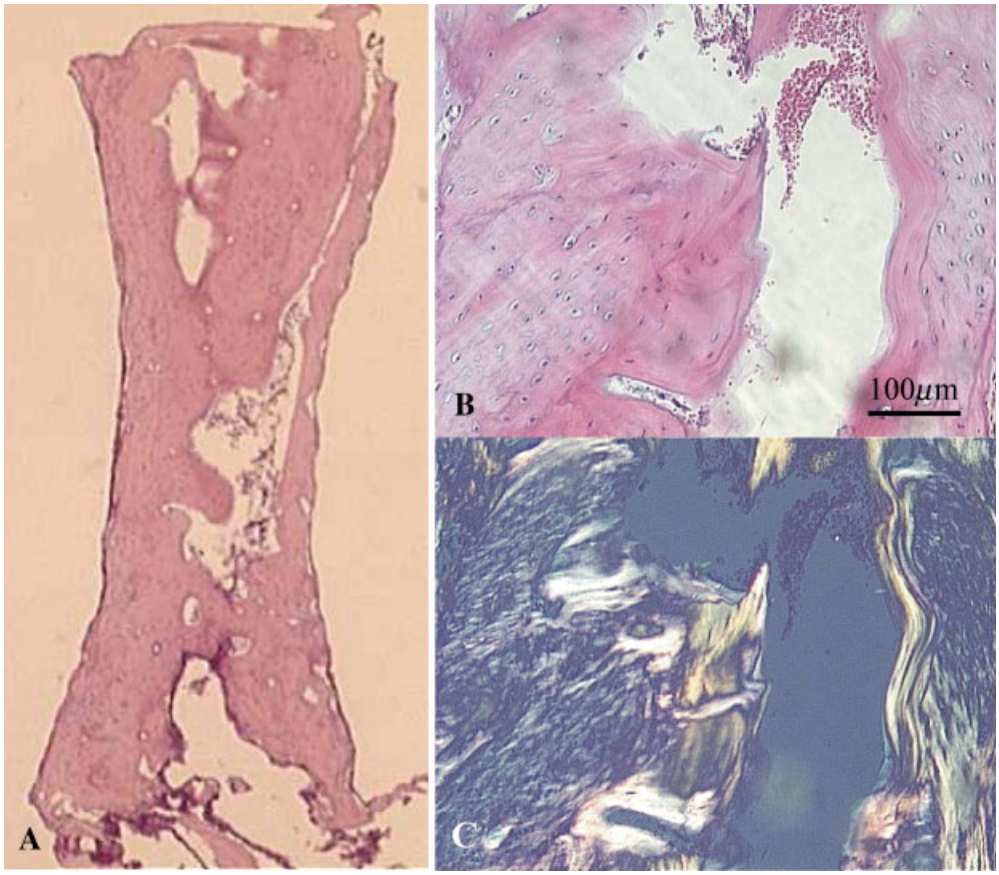

Figure 5. Representative 12 week explant. (A) Explant is 2.5 mm in length. Absence of blue staining indicated the absence of endochondral tissue. Note mixture of woven and lamellar tissues visible in (B) light and (C) polarized microscopy images. Original magnification ×100. [Color scheme can be viewed in the online issue, which is available at http://www.interscience.wiley.com]

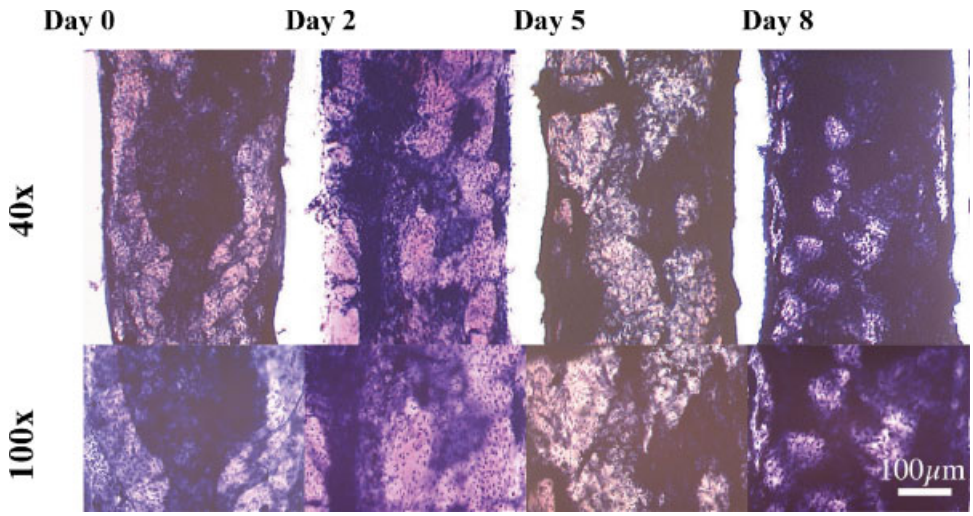

Figure 6. Osteocyte viability in culture as measured by L-lactate dehydrogenase (LDH) activity. Central gauge segments were shown at ×40 and ×100 original magnifications. Note discrete dark blue stained osteocytes indicating LDH activity. At ×40, gauge segments were 0.312″ wide. [Color scheme can be viewed in the online issue, which is available at http://www.interscience.wiley.com]

 DOI 10.1002/jor

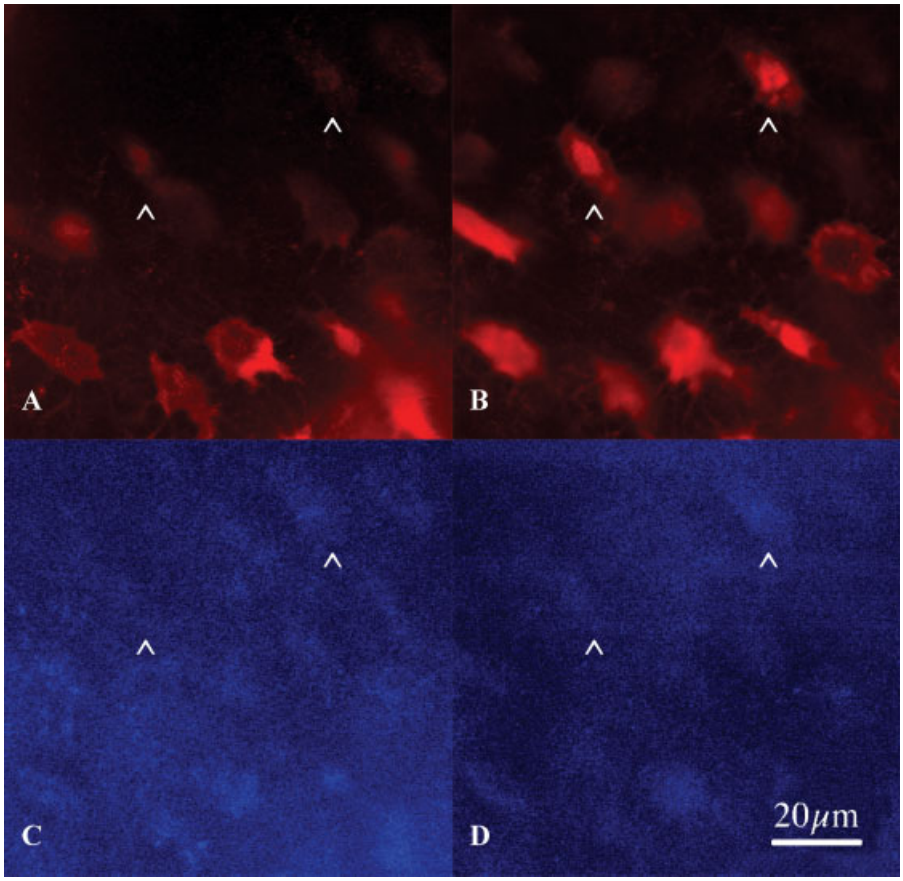

Figure 7. Representative diffusion temporal series. Explant incubated in 200 μM Alexa Fluor 633 hydrazide (~950 Da) using 633 nm excitation for (A) 10 min and (B) 120 min; and incubated in 200 μM Alexa Fluor 546 biocytin (1,209.7 Da) using 543 nm excitation for (C) 10 min and (D) 120 min. Laser scanning confocal data were collected ~45 μm from tissue surface with a 1.8 μm optical thickness at ×400 (original magnification). Two osteocyte lacunae were emphasized with arrowheads. [Color scheme can be viewed in the online issue, which is available at http://www.interscience.wiley.com]

activity.[32] We have developed, characterized, and demonstrated the feasibility of a system that maintained these critical osteocyte–ECM interactions and allowed investigations of the mechanoresponsiveness of individual osteocytes.

As implantation period increased from 6 to 12 weeks, explant bone tissue volume and mineralization trended upward and nearly doubled. A strong correlation between volumetric BMD and BV/TV suggested that, by 6 weeks, bone formation and mineralization were occurring simultaneously without allowing large volumes of osteoid to accumulate prior to mineralization. Specimen thickness only explained 14% of the variation in BV/TV suggesting that small manufacturing variations in implant geometry and compliance were not dictating tissue in-growth.

Eight-month-old 260–350 g female Sprague-Dawley rats were reported to have a BV/TV near 30% in intact proximal tibial metaphysis.[33] This value was slightly lower than values found in explants (38.5% at 12 weeks) and may have reflected differences in gender, weight, location, or tissue maturity. Matched literature values of BMD measured per unit volume were unavailable.

Bone tissue appeared to form via an intramembranous pathway based on morphologic analysis. However, the presence of occasional alcian blue staining indicated that cartilaginous molecular constituents might have been present in the absence of frank endochondral microstructure. Future immunohistochemical characterization of these tissues may improve our understanding of this process.

We have referred to the explant tissue as "native bone matrix" to emphasize that it was synthesized in vivo via endogenous mesenchyme and was responding physiologically to a pathologic but realistic insult. The tissue was primarily woven and not lamellar, which should be considered for

data interpretation. Given that intramembranous bone formation is central to bone embryology and fracture healing, the model could be more suited to explore these systems than fully remodeled lamellar bone.

While all bone cell types were present, adipocytes were absent and may have been compromised during histologic processing. Marrow cells were present, and their increased cellularity may have reflected that the bone originally developed from granulation tissue. The full complement of bone and hematologic cells suggested that this tissue may recapitulate the complex biology of bone regeneration. Such complex behaviors include stimulating osteoblastogenesis, osteoclastogenesis, and neovascularization.

Lamellar tissue area data indicated that explants did not mature to a predominantly lamellar microstructure. Quantitative analysis demonstrated a trend toward more lamellar tissue after 12 weeks of implantation. Although the standard deviation in lamellar tissue area at 12 weeks was more pronounced than that at earlier time points, a one-way ANOVA was used. The null difference result should be interpreted cautiously. At the least, the data suggested that there was more heterogeneity in lamellar bone synthesis at 12 weeks, possibly caused by a change in osteoblast activity.

When evaluating single osteocytes, their location within lamellar or woven tissue must be considered. As current studies were performed using confocal microscopy, this distinction could be readily accomplished by saturating fluorescence in cells labeled with intracellular probes to detail canaliculi. Lamellar osteocytes had a much more anisotropic canalicular network than woven bone osteocytes.[34] Another alternative was to restrict analysis to 10-week specimens where lamellar tissue values were smaller and more homogeneous.

The modest but significant correlation between specimen thickness and lamellar tissue area suggested that implant geometry can influence tissue maturation in this model. It was not certain whether the effect was due to implant compliance or the absolute size of the void for in-growth. Interpretation of these data was also complicated by surgical defect variation. The same surgeon performed all procedures for this study. While the procedure was reproducible, it lacked the manufacturing precision that would have made it possible to distinguish subtle influences of defect size, implant compliance, and host femur compliance.

Day 8 viability data suggested that tissues remained living ex vivo in tissue culture. Results not only validated the culture technique, but they support the assertion that explants were harvested with little trauma.

Polar tracer data suggested that at 200 μM, moieties greater than 1,200 Da could not be practically introduced using diffusion. Current 1,209.7 Da tracer data differ from Knothe-Tate et al.,[31] who found endosteal and periosteal evidence of microperoxidase (1,800 Da) diffusion in 60-day-old rats 2 h following injection. With intravascular volume estimated to be 5%–7% of body mass, the IV concentration of microperoxidase was approximately 1,700–2,300 μM. This concentration difference may have partially accounted for the discrepancy in results. Convective transport driven by cardiovascular pressure gradients may have also helped explain the difference.

Polar tracers were selected for their hydrophilic properties, which facilitated their diffusion in an aqueous environment. While the data described the time period required for polar tracers to access various microstructural compartments, the model may not have reflected biologic probe behavior in cell culture. First, reagents for intracellular measurements usually have hydrophobic components to facilitate passage across cell membranes. Regardless of solubilization with a detergent, the diffusion of actual probes would likely be slower than the polar tracer model. Second, while a given moiety may have accessed the lacunar space quickly, the additional time required for the probe to diffuse across a membrane was unknown. These shortcomings suggested that polar tracer models of diffusion may have underpredicted the time necessary for cell labeling for functional studies. Lastly, the probe molecular structure likely influenced diffusion as well, which may be detailed in future studies.

This model was limited by variability in specimen bone volume density and volumetric bone mineral density produced at various implantation periods. When compared to tissues samples cut from intact bone, this model offered the ability to harvest tissues with minimal trauma and reduce potential background mechanical stimulation, which might have complicated data interpretation. Additionally, this model may have left the native osteocyte network more intact than in samples that were cut from intact bone. With respect to harvested whole bone, this model offered the advantage of controlling specimen geometry, which could facilitate mechanical testing, microscopic imaging, and tissue culture.

Future investigations will use three-point bending to study real-time intracellular osteocyte pH as mechanical forces are applied to their mineralized extracellular matrix. Preliminary data suggest that the rectangular geometry of the explant can facilitate mechanical testing and provide a relatively flat surface that permits the confocal laser source to penetrate tens of microns into the sample.[35]

Further studies should also help discern whether pH changes during loading are caused by mechanotransduction or by load-induced fluid flow (transport) phenomena. In mechanotransduction, mechanical energy was applied to a cell and converted to biologic activity by the cell. Mechanotransduction can be distinguished from nutrient or electrolyte transport phenomena by the mechanism of mechanical energy conversion. If a biologic response was caused by altered nutrient transport, fluid motion changes the local chemical environment *independent* of the cell; i.e., the cell was not required for this process.[36,37] Subsequently, the cell would respond to this local chemical change and *not* the initial mechanical perturbation. The current model was not designed to explore the osteocyte's local fluid environment. However, mechanotransduction could be confirmed by demonstrating that loading response is abrogated when specific mechanotransduction organelles, like microfilaments, microtubules, or stretch-activated ion channels, were interrupted.

A model has been created that allows one to study osteocytes in the context of their native intact three-dimensional extracellular matrix and introduce intracellular probes to monitor real-time biologic activity of osteocytes. The model employed a well-tolerated, minimally traumatic, biocompatible implant system with a flexible geometry that permits growth of precisely shaped bone specimens. The implant–explant system tissue has been studied with micro computed tomography and histology to determine that it was a solid model of mostly intramembranous bone and likely capable of reproducing complex biologic processes in an appropriate environment. Explant viability in culture has been detailed along with practical diffusion information for introducing biologic probes. Preliminary studies are in progress to confirm that intracellular pH can be monitored during mechanical loading by measuring changes in relative fluorescence. Optical quantification of the mechanical environment around specific osteocytes may be possible given the flat surface of explant and optical penetration of confocal lasers. Future studies will include theoretical development and practical validation of optical methods to quantify perilacunar bone matrix strains. The implications of osteocyte pH changes secondary to mechanical stimulation will also be explored.

ACKNOWLEDGMENTS

The authors thank John Baker, Cari Bryant, Dr. Robert Dennis, Bruce Donahoe, Colleen Doyle, Chris Edwards, Dennis Kayner, Dr. Laurie McCauley, Bonnie Nolan, Charles Roehm, Dr. Mitchell Schaffler, Dotty Sorensen, Mark Stock, Kathy Sweet, and Peggy Piech for their respective contributions. This investigation was supported by the Arthritis Foundation and grants from the National Institutes of Health (Medical Scientist Training Program). Grant Numbers T32-GM07505, DK 070071, Institute of Gerontology Training Grant Number T32-AG00114 and the University of Michigan Musculoskeletal Core Center, Grant Number AR46024.

REFERENCES

1. Courtney AC, Hayes WC, Gibson LJ. 1996. Age-related differences in post-yield damage in human cortical bone. Experiment and model. J Biomech 29:1463–1471.
2. Schaffler MB, Boyce TM, Lundin-Cannon KD, et al. 1995. Age-related architectural change and microdamage accumulation in the human femoral neck cortex. In: Transactions of the 41th Annual Meeting of the Orthopaedic Research Society, p 549.
3. Schaffler MB, Choi K, Milgrom C. 1995. Aging and matrix microdamage accumulation in human compact bone. Bone 17:521–525.
4. Lips P. 1997. Epidemiology and predictors of fractures associated with osteoporosis. Am J Med 103:3S–8S.
5. Melton LJD, Cummings SR. 1987. Heterogeneity of age-related fractures: implications for epidemiology. Bone Miner 2:321–331.
6. Carter DR, Hayes WC. 1977. Compact bone fatigue damage: a microscopic examination. Clin Orthop Relat Res 127:265–274.
7. Chamay A. 1970. Mechanical and morphological aspects of experimental overload and fatigue in bone. J Biomech 3:263–270.
8. Mori S, Harruff R, Ambrosius W, et al. 1997. Trabecular bone volume and microdamage accumulation in the femoral heads of women with and without femoral neck fractures. Bone 21:521–526.
9. Noble BS, Stevens H, Mosley JR, et al. 1997. Bone loading changes the number and distribution of apoptotic osteocytes in cortical bone (abstract). J Bone Miner Res 12:36.
10. Verborgt O, Gibson GJ, Schaffler MB. 2000. Loss of osteocyte integrity in association with microdamage and bone remodeling after fatigue in vivo. J Bone Miner Res 15:60–67.
11. Fox SW, Chambers TJ, Chow JW. 1996. Nitric oxide is an early mediator of the increase in bone formation by mechanical stimulation. Am J Physiol 270:E955–E960.
12. Lean JM, Jagger CJ, Chambers TJ, et al. 1995. Increased insulin-like growth factor I mRNA expression in rat

osteocytes in response to mechanical stimulation. Am J Physiol 268:E318–E327.
13. O'Connor JA, Lanyon LE, MacFie H. 1982. The influence of strain rate on adaptive bone remodelling. J Biomech 15: 767–781.
14. Rubin CT, Lanyon LE. 1984. Regulation of bone formation by applied dynamic loads. J Bone Joint Surg [Am] 66:397–402.
15. Rubin CT, Sun YQ, Hadjiargyrou M, et al. 1999. Increased expression of matrix metalloproteinase-1 in osteocytes precedes bone resorption as stimulated by disuse: evidence for autoregulation of the cell's mechanical environment? J Orthop Res 17:354–361.
16. Sun Y-Q, McLeod KJ, Rubin CT. 1995. Mechanically induced periosteal bone formation is paralleled by the upregulation of collagen type one mRNA in osteocytes as measured by in situ reverse transcript-polymerase chain reaction. Calcif Tissue Int 57:456–462.
17. Bentolila V, Boyce TM, Fyhrie DP, et al. 1998. Intracortical remodeling in adult rat long bones after fatigue loading. Bone 23:275–281.
18. Lanyon LE, Goodship AE, Pye CJ, et al. 1982. Mechanically adaptive bone remodelling. J Biomech 15:141–154.
19. Noble BS, Reilly GC, Peet N, et al. 2003. Mechanical loading: biphasic osteocyte survival and targeting of osteoclasts for bone destruction in rat cortical bone. Am J Physiol Cell Physiol 284:C934–C943.
20. Tang LY, Cullen DM, Yee JA, et al. 1997. Prostaglandin E2 increases the skeletal response to mechanical loading. J Bone Miner Res 12:276–282.
21. Torrance AG, Mosley JR, Suswillo RF, et al. 1994. Noninvasive loading of the rat ulna in vivo induces a strain-related modeling response uncomplicated by trauma or periostal pressure. Calcif Tissue Int 54:241–247.
22. Turner CH, Akhter MP, Raab DM, et al. 1991. A noninvasive, in vivo model for studying strain adaptive bone modeling. Bone 12:73–79.
23. Dallas SL, Zaman G, Pead MJ, et al. 1993. Early strain-related changes in cultured embryonic chick tibiotarsi parallel those associated with adaptive modeling in vivo. J Bone Miner Res 8:251–259.
24. Pitsillides A, Rawlinson SC, Suswillo RF, et al. 1995. Mechanical strain-induced NO production by bone cells: a possible role in adaptive bone (re)modeling? FASEB J 9:1614–1622.
25. Rawlinson SC, Mosley JR, Suswillo RF, et al. 1995. Calvarial and limb bone cells in organ and monolayer culture do not show the same early responses to dynamic mechanical strain. J Bone Miner Res 10:1225–1232.
26. Rawlinson SC, Pitsillides AA, Lanyon LE. 1996. Involvement of different ion channels in osteoblasts' and osteocytes' early responses to mechanical strain. Bone 19:609–614.
27. Rawlinson SC, Zaman G, Mosley JR, et al. 1998. Heme oxygenase isozymes in bone: induction of HO-1 mRNA following physiological levels of mechanical loading in vivo. Bone 23:433–436.
28. Zaman G, Pitsillides AA, Rawlinson SC, et al. 1999. Mechanical strain stimulates nitric oxide production by rapid activation of endothelial nitric oxide synthase in osteocytes. J Bone Miner Res 14:1123–1131.
29. Corboz VA, Cecchini MG, Felix R, et al. 1992. Effect of macrophage colony-stimulating factor on in vitro osteoclast generation and bone resorption. Endocrinology 130: 437–442.
30. Wong SYP, Dunstan CR, Evans RA, et al. 1982. The determination of bone viability: a histochemical method for identification of lactate dehydrogenase activity in osteocytes in fresh calcified and decalcified sections of human bone. Pathology 14:439–442.
31. Knothe-Tate ML, Niederer P, Knothe U. 1998. In vivo tracer transport through the lacunocanalicular system of rat bone in an environment devoid of mechanical loading. Bone 22:107–117.
32. Cukierman E, Pankov R, Stevens DR, et al. 2001. Taking cell-matrix adhesions to the third dimension. Science 294:1708–1712.
33. Takahashi M, Wehrli FW, Wehrli SL, et al. 1999. Effect of prostaglandin and bisphosphonate on cancellous bone volume and structure in the ovariectomized rat studied by quantitative three-dimensional nuclear magnetic resonance microscopy. J Bone Miner Res 14:680–689.
34. Remaggi F, Cane V, Palumbo C, et al. 1998. Histomorphometric study on the osteocyte lacuno-canalicular network in animals of different species. I. Woven-fibered and parallel-fibered bones. Ital J Anat Embryol 103:145–155.
35. Hoffler CE, Doyle CM, Bryant CR, et al. 2004. A new model to study osteocyte bone matrix interactions in real-time. In: Transactions of the 50th Annual Meeting of the Orthopaedic Research Society, San Francisco, CA; p 508.
36. Knothe Tate ML, Steck R, Forwood MR, et al. 2000. In vivo demonstration of load-induced fluid flow in the rat tibia and its potential implications for processes associated with functional adaptation. J Exp Biol 203:2737–2745.
37. Tami AE, Nasser P, Verborgt O, et al. 2002. The role of interstitial fluid flow in the remodeling response to fatigue loading. J Bone Miner Res 17:2030–2037.